ORIGINAL PAPER

A tunable optofluidic lens based on combined effect of hydrodynamics and electroosmosis

Haiwang Li · Teck Neng Wong · Nam-Trung Nguyen

Abstract This paper presents the modeling and experimental results of a liquid-core liquid-cladding optofluidic lens under the combined effect of hydrodynamics and electroosmosis. To allow the lens to be tuned by a voltage, the cladding fluids are electrically conducting, while the core fluid is non-conducting. Under constant flow rates, mathematical models of two-dimensional dipole flow in a circularly bounded domain and electric field outside the parallel-plate capacitor were used to predict the curvature of the interface. A test device with a circular lens chamber with 2 mm diameter and 250 μm height was fabricated in polymethylmethacrylate (PMMA) using thermal bounding method. Two cladding fluids (aqueous NaCl) and the core fluid (silicone oil) are introduced into the circular domain by syringe pumps. External electric fields are applied on the two cladding fluids. Under the same inlet volumetric flow rates, the applied voltages are varied to tune the curvature of the interfaces between the cladding fluids and the core fluid. The interface shape is measured using fluorescence imaging technique. The results show that the interfaces between the cladding fluids and the core fluid have optically smooth arc shape. Under fixed cladding flow rates, the same voltage forms symmetric biconvex lens only. Different voltages can form biconvex lens, plano-convex lens, and meniscus lens. The experimental results agree well with the presented analytical model.

Keywords Optofluidics · Interface · Microlens · Hydrodynamic · Electroosmosis

H. Li · T. N. Wong (✉) · N.-T. Nguyen
School of Mechanical and Aerospace Engineering,
Nanyang Technological University, 50 Nanyang Avenue,
Singapore 639798, Singapore
e-mail: mtnwong@ntu.edu.sg

1 Introduction

Microlenses are widely integrated into lab-on-a-chip (LOC) systems to improve the portability of optical components and make the system cost-effective (Camou et al. 2003; Wenger et al. 2008). However, the focal length of the solid lens is not tunable and the smoothness of interface of the solid lens depends on the fabrication process. Micro optofluidics, which combines the fields of microfluidics and microoptics, is implemented by controlling liquid interfaces in microchannels. Fluids have unique properties that cannot be found in solid equivalents, and these properties can be used to design novel optical components. These properties are: (1) the optical property can be changed by simple replacing one fluids with another; (2) interface between two immiscible fluids is smooth; (3) the miscible fluids can create gradient in optical properties by diffusion (Psaltis et al. 2006); (4) finer features is possible to be achieved in the composed fluid media (Psaltis et al. 2006). In microfluidic devices, the flows are always laminar due to the small size of the devices (Weigl et al. 2001). Under laminar conditions in a micro device, the interfaces between different fluids is stable and smooth, thus ideal for designing optical components such as waveguides, lenses, and mirrors (Wolfe et al. 2004).

Recently, the development of optofluidic lens has attracted interests from the microfluidics research community (Dino 2009; Rosenauer and Vellekoop 2009; Shi et al. 2010). To enhance the optical performance, Dong and Jiang (2008) formed an in situ tunable liquid microlens using liquid–air interfaces of liquid droplets. To further demonstrate the potential of using the liquid microlenses, Liu et al. (2009) formed microlens arrays with separate tunable microlenses. Unfortunately, complex structure and controlling procedures limited the application potential of

this method. When the liquids flow through a 90-degree curve in a microchannel, the centrifugal effect causes the fluidic interface to bend. Utilizing this effect, Mao et al. (2007, 2008, 2009) designed normal refractive lens (Mao et al. 2007) and gradient refractive index (GRIN) lens (Mao et al. 2008, 2009), respectively. The shape of the interface is difficult to control accurately using this method. Tang et al. (2008) and Song et al. (2009) designed liquid-core liquid-cladding optofluidics lenses based on three laminar streams in PDMS rectangular and circular chambers. The curvature of these lenses can be tuned by the flow rate ratios of the three stream (Nguyen 2010; Song et al. 2010).

Electroosmosis is one of the most popular actuation methods in microfluidics (Manz et al. 1994; Ren et al. 2001; Sinton and Li 2003; Kohlheyer et al. 2005; Li et al. 2009). Compared to pressure-driven methods, electroosmosis has many advantages in tuning an optofluidic lens. For example, the flow rate ratio between the cladding flows and the core flow is too high when the curvature is large. Electroosmotic flow has a wide range of applications as it has a uniform flow velocity profile and no moving parts. In microsystems, surface-to-volume ratio is large; electroosmosis will be more efficient than ordinary pressure-driven flow.

This paper presents a new design of a circular chamber to realize an optically smooth lens curvature; the curvature can be adjusted using the combined effect of pressure driven and electroosmosis. Figure 1 shows the schematic concept of this optofluidic lens. The two cladding streams (cladding fluid 1 and cladding fluid 3) are electrically conducting with high electroosmotic mobility, while the core stream (core fluid 2) is non-conducting with low electroosmotic mobility. At a given pressure gradient and voltages applied along the conducting cladding fluids, electroosmotic forces control the curvature of the interfaces (interface 1–2 and interface 3–2) between the conducting cladding fluids and the core fluid. The curvatures of the interfaces depend on the directions and magnitudes of the applied voltages.
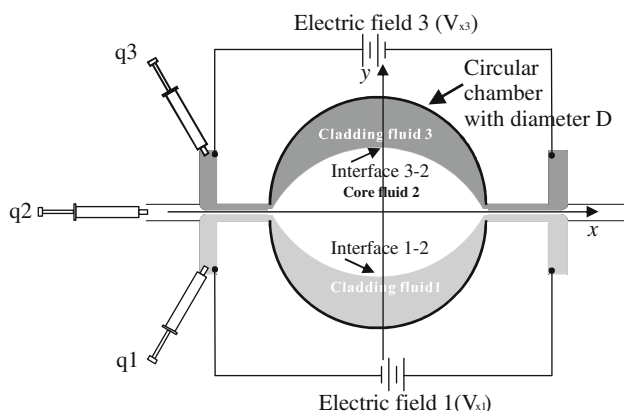

Fig. 1 Schematic representation of the optofluidics lens under the combined effect of hydrodynamic and electroosmosis

This paper focuses on the fluidic aspect of the lens design under the combined effect of pressure-driven flow and electroosmotic flow. Optical characteristics of this lens should be similar to that of a lens tunable by pressure-driven flow as reported in details by Song et al. (2010). First, the theories, including two-dimensional dipole flow in a circularly bounded domain and the electric field outside a parallel-plate capacitor, are used to establish the interface shape. Second, the paper derives the relationships between the curvature of the interface and the combined effect of the flow rate ratio of the core/cladding streams and the electric fields in the cladding fluids. Finally, experiments were carried out to verify the theory.

2 Analytical model

Li et al. (2009) showed the concept of using electroosmotic control of width and position of liquid streams in hydrodynamic focusing. Hence the velocity field of the optofluidic lens shown in Fig. 1 can be decomposed into two parts,

$$\begin{cases} u = u^p + u^E \\ v = v^p + v^E \end{cases} \tag{1}$$

where u and v are the velocities along x and y-axes, respectively. The superscripts E and p denote the velocity components caused by electroosmotic forces and the pressure gradient, respectively. In the following parts, the velocities and flow rates caused by hydrodynamics and electroosmosis will be derived separately.

2.1 Hydrodynamic velocity

In Fig. 1, relative to the diameter of the circular chamber, D, the widths of the inlet and outlet are so small that they can be assumed as a source (inlet) and a sink (outlet). The total flow rate of three flows is regarded as the strength of the source and the sink. The model can be assumed as the source–sink pair model. From Koplik et al. (1994) and Song et al. (2009), a source of strength Q is placed at $(R, 0)$ in Cartesian coordinates, and a corresponding sink of strength $-Q$ is located at $(-R, 0)$ (Fig. 2). The source/sink strength, Q, represents the total flow rate entering/exiting the chamber. The field can be described by the complex potential:

$$\begin{aligned} W(z) &= \phi + i\psi \\ &= \frac{Q}{2\pi}\big[\log(z + R) - \log(z - R) + \log(R^2 + Rz) \\ &\quad - \log(R^2 - Rz)\big] \end{aligned} \tag{2}$$

where ϕ is the velocity potential, ψ is the stream potential, i is the imaginary unit, $z = x + iy$, x and y are the
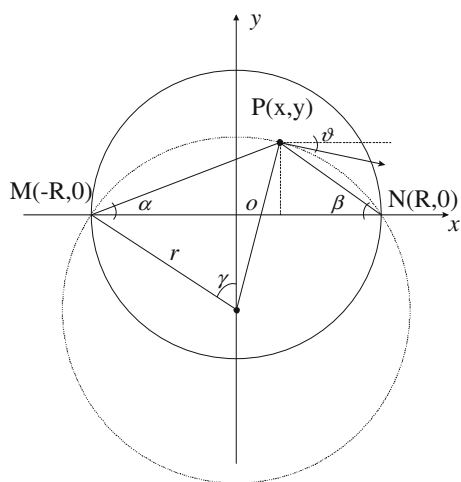
Fig. 2 Schematic representation of the theory of two-dimensional dipole flow in a circularly bounded domain

coordinates in the two-dimensional Cartesian system, and R is the radius of the circular domain. The term of Eq. 2 can be described as follows:

$$z + R = (x + R) + yi = \sqrt{(x+R)^2 + y^2} \times e^{i\theta} \quad (3)$$

According Fig. 1, θ can be described

$$\theta = \tan^{-1}\left(\frac{y}{x+R}\right) \quad (4)$$

Substituting Eqs. 3 and 4 into Eq. 2, the terms of Eq. 2 transforms into

$$\log(z+R) = \log\left[\sqrt{(x+R)^2+y^2} \times e^{i\theta}\right]$$
$$= \log\sqrt{(x+R)^2+y^2} + i\tan^{-1}\left(\frac{y}{x+R}\right) \quad (5)$$

$$\log(z-R) = \log\left[\sqrt{(x-R)^2+y^2} \times e^{i\theta}\right]$$
$$= \log\sqrt{(x-R)^2+y^2} + i\tan^{-1}\left(\frac{y}{x-R}\right) \quad (6)$$

$$\log(R^2 + Rz) = \log\left[\sqrt{(R^2+Rx)^2+(Ry)^2} \times e^{i\theta}\right]$$
$$= \log\sqrt{(R^2+Rx)^2+(Ry)^2} + i\tan^{-1}\left(\frac{y}{x+R}\right) \quad (7)$$

$$\log(R^2 - Rz) = \log\left[\sqrt{(R^2-Rx)^2+(Ry)^2} \times e^{i\theta}\right]$$
$$= \log\sqrt{(R^2-Rx)^2+(Ry)^2} + i\tan^{-1}\left(\frac{y}{R-x}\right) \quad (8)$$

Substituting Eqs. 5–8 into Eq. 2, the real part of Eq. 2 is

$$\psi = \tan^{-1}\left(\frac{y}{x+R}\right) - \tan^{-1}\left(\frac{y}{x-R}\right) + \tan^{-1}\left(\frac{y}{x+R}\right)$$
$$- \tan^{-1}\left(\frac{y}{R-x}\right)$$
$$= 2\tan^{-1}\left(\frac{y}{x+R}\right) + 2\tan^{-1}\left(\frac{y}{R-x}\right) - \pi \quad (9)$$

The streamlines are a cluster of curves $\psi = C_i$. The point (x, y) at each streamline should satisfy the following equation:

$$\tan^{-1}\left(\frac{y}{x+R}\right) + \tan^{-1}\left(\frac{y}{R-x}\right) = \frac{C_i + \pi}{2} \quad (10)$$

For each specific C_i, Eq. 10 defines a curve representing a streamline.

According the properties of stream function,

$$u^p = \frac{\partial \psi}{\partial y} \quad (11)$$

$$v^p = -\frac{\partial \psi}{\partial x} \quad (12)$$

Combining Eqs. 2–12, the velocity can be described as

$$u^p = \frac{Q}{2\pi}\left[\frac{2(x+R)}{(x+R)^2+y^2} - \frac{2(x-R)}{(x-R)^2+y^2}\right] \quad (13)$$

$$v^p = \frac{Q}{2\pi}\left[\frac{2y}{(x+R)^2+y^2} - \frac{2y}{(x-R)^2+y^2}\right] \quad (14)$$

At the center line of the circular domain, $x = 0$, Eqs. 13 and 14 reduce to

$$\begin{cases} u^p = \dfrac{2QR}{\pi(R^2 + y^2)} \\ v^p = 0 \end{cases} \quad (15)$$

The detailed mathematical derivation of pressure driven velocity is similar with Song et al. (2010)

2.2 Electric field

In a straight microchannel, the electric field between two electrodes is similar to that of a parallel-plate capacitor. In a circular chamber, we assume that the electric field is the outside electric field of finite-size parallel electrodes. With reference to Ren and Liu (2007), the electric field can be derived using the following method.

Figure 3 shows the model of the electric field outside a parallel capacitor. To analyze this model, a Cartesian coordinate system (x, y) is used where the origin point, O $(0, 0)$, is set at the center of the parallel plates capacitor. The electric field of point P (x, y) (Fig. 3) is the coupled effect of the cell area of positive electrode, dS_2 (R, y''), and the cell area of negative electrode, dS_1. The
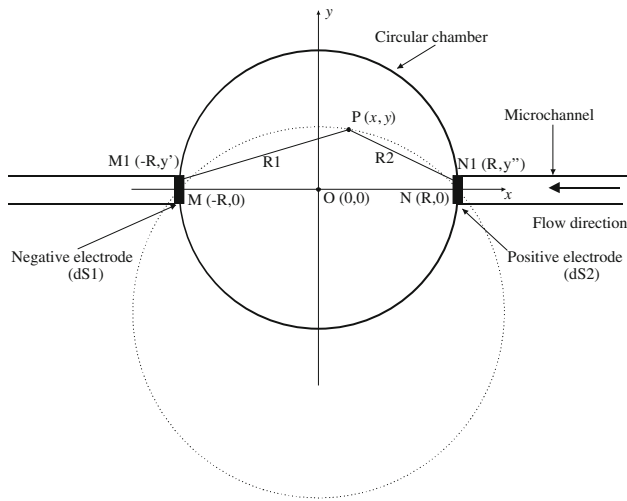
Fig. 3 Schematic representation of the theory of the electric field outside the parallel capacitor

superscripts $'$ and $''$ describe the negative electrode and the positive electrode, respectively. M_1 $(-R, y')$ is one arbitrary point on the negative electrode, and N_1 (R, y'') is one arbitrary point on the positive electrode. R_1 and R_2 are the distances between P (x, y) and any points belonging to the two plates, can be described as

$$R_1 = \sqrt{(R+x)^2 + (y-y')^2} \tag{16}$$

$$R_2 = \sqrt{(x-R)^2 + (y-y')^2} \tag{17}$$

where R is the radius of the circular chamber. Equation 18 shows the relationship between the strength of electric field and the density of the charge:

$$\frac{4\pi\varepsilon V_0}{2} = \oint_{S_1} \frac{\sigma(-R, y')dS_1(-R, y')}{R_1} + \oint_{S_2} \frac{\sigma(R, y'')dS_2(R, y'')}{R_2} \tag{18}$$

where σ $(-R', y')$ is the density of charge on the surface of the negative electrode, σ (R'', y'') is the density of charge on the surface of the positive electrode, ε is the permittivity of the fluid, and V_0 is the voltage between the electrodes. Because σ $(-R', y')$ and σ (R'', y'') have the same magnitudes but opposite polarities, Eq. 18 transforms into

$$\sigma(-R, y) = \frac{2\pi\varepsilon V_0}{\oint_{S_1} \frac{dS_1(-R, y')}{R_1} - \oint_{S_2} \frac{dS_2(R, y'')}{R_2}} \tag{19}$$

The electric field between two points can be described as

$$dE = \frac{\sigma(-R, y)dS_1(-R, y')}{4\pi\varepsilon r^2} \tag{20}$$

where r is the distance between P (x, y) and M_1 $(-R, y')$, P is a point between two electrodes, r can be described as

$$r^2 = R_1^2 = (R+x)^2 + (y-y')^2 \tag{21}$$

For P $(0, y)$, substituting Eq. 21 into Eq. 20, the electric field can be described

$$E_p = \frac{d\sigma(-R, y)}{4\pi\varepsilon} \int_{-Y_1}^{Y_1} \frac{1}{\left[(R+x)^2 + (y-y')^2\right]^{\frac{3}{2}}} dy \tag{22}$$

where $-Y_1$ is the lower edge of the electrodes and Y_1 is the upper edge of the electrodes. The velocity under the effect of electroosmosis can be described using the Helmholtz-Smoluchowski electroosmotic velocity

$$\begin{cases} u^E = \dfrac{E_x \varepsilon \xi}{\mu} \\ v^E = \dfrac{E_y \varepsilon \xi}{\mu} \end{cases} \tag{23}$$

where E_x and E_y are the electric fields along the respective axis, ξ is the zeta potential of the surface, and μ is the dynamic viscosity of the fluid. Using Eq. 23, the electroosmotic velocities at the center line of the cladding fluids are

$$\text{(cladding fluid 1)} \begin{cases} u_1^E = \dfrac{\xi_1 \varepsilon_1 E_{x1}}{\mu_1} \\ v_1^E = 0 \end{cases} \tag{24}$$

and

$$\text{(cladding fluid 3)} \begin{cases} u_3^E = \dfrac{\xi_3 \varepsilon_3 E_{x3}}{\mu_3} \\ v_3^E = 0 \end{cases} \tag{25}$$

For the core fluid, there is no electroosmotic effect; the electroosmotic velocity can be modeled from the Navier–Stokes equation:

$$\frac{\partial(\rho u^E)}{\partial t} + \nabla \cdot (\rho u^E u^E) = \mu\left(\frac{\partial^2 u^E}{\partial x^2} + \frac{\partial^2 u^E}{\partial y^2}\right) \tag{26}$$

For steady one-dimension fully developed flow, Eq. 26 reduces into

$$\frac{d^2 u^E}{dy^2} = 0 \tag{27}$$

According Eq. 27, the velocity u can be assumed as

$$u^E = C_1 y + C_2 \tag{28}$$

The boundary conditions of Eq. 28 is

$$\begin{cases} u^E = \dfrac{\xi_1 \varepsilon_1 E_{x1}}{\mu_1} & \text{at } y = B_2, \text{ position of interface } 1-2 \text{ (Fig.4)} \\ u^E = \dfrac{\xi_3 \varepsilon_3 E_{x3}}{\mu_3} & \text{at } y = A_2, \text{ position of interface } 3-2 \text{ (Fig.4)} \end{cases} \tag{29}$$

where A_2 and B_2 are the y-positions of interface 3–2 and interface 1–2 at the origin, O, as shown in Fig. 4,
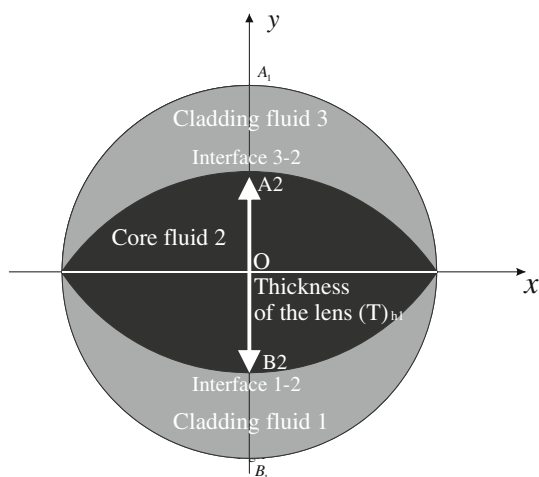
Fig. 4 The interface positions of a lens

respectively. The magnitudes of electric field, E_{x1} and E_{x3}, can be calculated using the following equations:

$$E_{x1} = \frac{d\sigma(-R,y)}{4\pi\varepsilon} \int_{-Y_1}^{Y_1} \frac{1}{\left[R^2 + (y + B_2)^2\right]^{\frac{3}{2}}} dy \tag{30}$$

$$E_{x3} = \frac{d\sigma(-R,y)}{4\pi\varepsilon} \int_{-Y}^{Y_1} \frac{1}{\left[(y - A_2)^2 + R^2\right]^{\frac{3}{2}}} dy \tag{31}$$

The positions of the interface, A_2 and B_2, can be calculated using the equations

$$B_2 = \sqrt{r_2^2 - R^2} - r_2 \tag{32}$$

$$A_2 = r_1 - \sqrt{r_1^2 - R^2} \tag{33}$$

where r_1 and r_2 are the radius of interface 1–2 and interface 3–2, respectively. Using the boundary conditions, Eq. 28 can be solved

$$u_2^E = \frac{\xi_1\varepsilon_1(\mu_3 E_{x1} - \mu_1 E_{x3})}{\mu_1\mu_3(B_2 - A_2)} y + \frac{\xi_3\varepsilon_3(\mu_3 E_{x1} A_2 - \mu_1 E_{x3} B_2)}{\mu_1\mu_3(A_2 - B_2)} \tag{34}$$

Hence the electroosmotic velocity can be described as (core fluid 2)

$$\begin{cases} u_2^E = \dfrac{\xi_1\varepsilon_1(\mu_3 E_{x1} - \mu_1 E_{x3})}{\mu_1\mu_3(B_2 - A_2)} y + \dfrac{\xi_3\varepsilon_3(\mu_3 E_{x1} A_2 - \mu_1 E_{x3} B_2)}{\mu_1\mu_3(A_2 - B_2)} \\ v_2^E = 0 \end{cases} \tag{35}$$

for core fluid 2.

The thickness of the lens is defined as (Fig. 4)

$$T_{h1} = A_2 - B_2 \tag{36}$$

The dimensionless lens thickness is defined as

$$\bar{T}_{h1} = \frac{T_{h1}}{D} \tag{37}$$

where D is the diameter of the circular chamber as shown in Fig. 1.

2.3 Flow rate

The volumetric flow rate through the microchannel can be defined by

$$q = q^E + q^p = \int_l u^E dy + \int_l u^p dy \tag{38}$$

where l is the width of the fluids along y-axis. From Eq. 38, the flow rates of the cladding fluid 1, the core fluid 2 and the cladding fluid 3 can be described as

$$q_1 = q_1^E + q_1^p = \int_{B_1}^{B_2} u_1^E dy + \int_{B_1}^{B_2} u_1^p dy \tag{39}$$

$$q_2 = q_2^E + q_2^p = \int_{B_2}^{A_2} u_2^E dy + \int_{B_2}^{A_2} u_2^p dy \tag{40}$$

$$q_3 = q_3^E + q_3^p = \int_{A_1}^{A_2} u_3^E dy + \int_{A_1}^{A_2} u_3^p dy \tag{41}$$

From Eqs. 15 and 24, the velocity at the center line for the cladding fluid 1 can be described as

$$\begin{cases} u_1^p = \dfrac{2QR}{\pi(R^2 + y^2)} \\ u_1^E = \dfrac{\xi_1\varepsilon_1 E_{x1}}{\mu_1} \end{cases} \tag{42}$$

For the core fluid 2, the velocity can be described as

$$\begin{cases} u_2^p = \dfrac{2QR}{\pi(R^2 + y^2)} \\ u_2^E = \dfrac{\xi_1\varepsilon_1(\mu_3 E_{x1} - \mu_1 E_{x3})}{\mu_1\mu_3(B_2 - A_2)} \cdot y + \dfrac{\xi_3\varepsilon_3(\mu_3 E_{x1} A_2 - \mu_1 E_{x3} B_2)}{\mu_1\mu_3(A_2 - B_2)} \end{cases} \tag{43}$$

For the cladding fluid 3, the velocity can be described as

$$\begin{cases} u_3^p = \dfrac{2QR}{\pi(R^2 + y^2)} \\ u_3^E = \dfrac{\xi_3\varepsilon_3 E_{x3}}{\mu_3} \end{cases} \tag{44}$$

Substituting Eqs. 42–44 into Eqs. 39–41, the flow rates are

$$q_1^E = \frac{\xi_1 \varepsilon_1 V_{x1}}{2R\mu_1} \int_{B_1}^{B_2} \frac{\sin(\alpha + \beta)}{(\alpha + \beta)} dy \tag{45}$$

$$q_1^P = \frac{2Q}{\pi}\left[\tan^{-1}\left(\left(\sqrt{r_2^2 - R^2} - r_2\right)\Big/R\right) + \frac{\pi}{4}\right] \tag{46}$$

$$q_2^E = \frac{\xi_1 \varepsilon_1 (\mu_1 E_{x3} - \mu_3 E_{x1})(A_2 + B_2)}{2\mu_1 \mu_3} + \frac{\xi_3 \varepsilon_3 (\mu_1 E_{x3} B_2 - \mu_3 E_{x1} A_2)}{\mu_1 \mu_3} \tag{47}$$

$$q_2^p = \frac{2Q}{\pi}\left[\tan^{-1}\left(\left(r_1 - \sqrt{r_1^2 - R^2}\right)\Big/R\right) - \tan^{-1}\left(\left(\sqrt{r_2^2 - R^2} - r_2\right)\Big/R\right)\right] \tag{48}$$

$$q_3^E = \frac{\xi \varepsilon V_{x3}}{2R\mu_3} \int_{A_1}^{A_2} \frac{\sin(\alpha + \beta)}{(\alpha + \beta)} dy \tag{49}$$

$$q_3^p = \frac{2Q}{\pi}\left[\frac{\pi}{4} - \tan^{-1}\left(\left(r_1 - \sqrt{r_1^2 - R^2}\right)\Big/R\right)\right] \tag{50}$$

where α and β are defined in Fig. 2 as: $\sin \alpha = \frac{y}{x+R}$ and $\sin \beta = \frac{y}{R-x}$.

2.4 Definitions of curvature

We define the field of the core fluid 2 as a region, the interface 1–2 and interface 3–2 are the boundaries of the region, and the curvature of the interface is defined as the divergence of the normal of the interface. The symbol of the curvatures can be defined as $\kappa > 0$ for the convex region and $\kappa < 0$ for the concave region (Fig. 5).

The curvature of interface 1–2 (κ_{1-2}) and the curvature of the interface 3–2 (κ_{3-2}) can be calculated using the following formula (Fig. 2):

$$\begin{cases} \kappa_{1-2} = -\dfrac{2B_2}{B_2^2 + R^2} \\ \kappa_{3-2} = \dfrac{2A_2}{A_2^2 + R^2} \end{cases} \tag{51}$$

3 Experiment

3.1 Materials and fabrication

Figure 6 shows the setup used in the experiment. Polymethylmethacrylate (PMMA) was used in our experiments as the substrate material because of its relatively high zeta potential suitable for electrokinetic control and the easy fabrication using laser micro machining. Thermal bonding technique is used to fabricate the microchannel. In this method, two PMMA plates (50 mm × 50 mm × 1 mm)
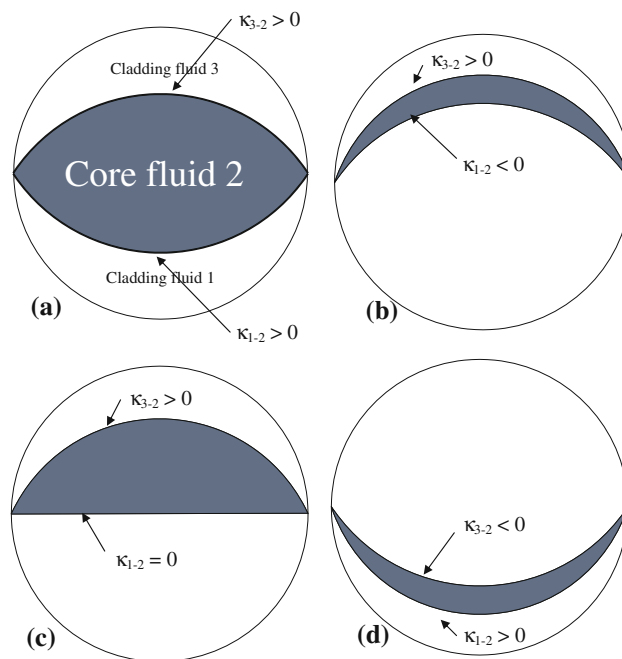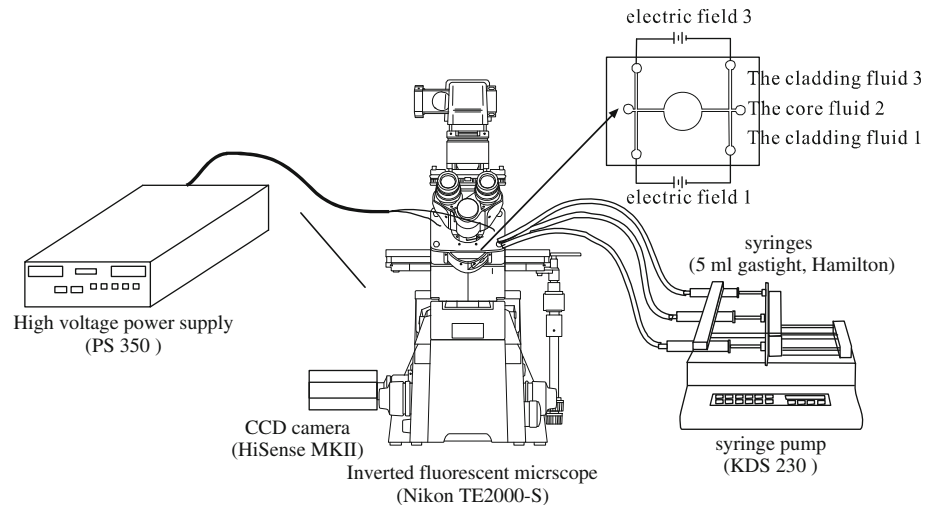

Fig. 5 The definition of the symbol of curvature and the model of lens. The core fluid is regarded as a region. Convex region has $\kappa > 0$, concave region has $\kappa < 0$, and a plan has $\kappa = 0$. **a** Biconvex lens, **b** meniscus lens; **c** plano-convex lens; **d** meniscus lens

and a PMMA film (50 mm × 50 mm × 250 μm) are bonded together. First, the two PMMA plates are cut using a CO_2 laser. Fluidic access holes and alignment holes are laser-machined into the PMMA substrate. Next, a PMMA film is cut to form the intermediate layer with the channel structures. The adhesive layer thickness of 250 μm defines the channel height. The three layers are positioned with alignment holes and bonded together. The process of thermal bonding is as follows. First, the PMMA layers were placed on the plate of a hot press (CARVER MANUAL PRESS 4386). Second, a pressure of 1.96×10^6 Pa was applied on the PMMA layers. Third, the temperature of 438 K was set. Using this thermal bonding process, an optofluidic lens with the chamber diameter of 2 mm and channel width of 100 μm was fabricated. As shown in Fig. 1, the three fluids flow side by side in the straight microchannel in the direction from left to right. The flows at the inlets are driven by syringe pumps. The outlets are connected to a waste reservoir. Voltages are applied by inserting two pairs of platinum electrodes.

3.2 Chemical and experimental setup

In our experiment, the cladding liquid is aqueous NaCl solution (7×10^{-4} M). Rhodamine B ($C_{28}H_{31}N_2O_3Cl$) was added to the NaCl solution at a concentration of 1 g/l. The viscosity of the NaCl solution was subsequently measured as 0.85×10^{-3} N s m^{-2}. The value of the

Fig. 6 The setup of the experiment

conductivity 86.6 µS/cm was taken from Yaws (2003). Rhodamine B was used by Wang et al. (2005) for visualizing coupled pressure-driven/electrokinetic flow and showed negligible effect on the flow itself. Rhodamine B is sensitive to temperature increase generated by Joule heating in the later experiments. However, it serves well for visualization purpose reported in this paper. The core fluid is silicone oil (Sigma-Aldrich), the viscosity and the density of the silicone oil is 1 cSt and 0.82 g/ml. The cladding liquid 1, the cladding liquid 3, and the core liquid 2 are pushed into the microchannel using three identical syringes (5 ml gastight, Hamilton) separately. The syringes are driven by a single syringe pump (Cole-Parmer, 74900-05, 0.2 µl/h to 500 l/h, accuracy of 0.5%).

A high voltage power supply (Model PS350, Stanford Research System, Inc) is used to provide the controlling voltages. The power supply is capable of producing up to 5000 V and changing the polarity of the voltage. The platinum wire is used as electrode. An interline transfer CCD camera (Sony ICX 084) attached to the microscope is used to capture the fluorescent images.

4 Results and discussion

In the experiment, the flow rates of cladding fluids and core fluid are kept constant ($q_1 = q_2 = q_3 = 0.05$ ml/h); the voltages (V_{x1} and V_{x3}) are modified using the high voltage power supply.

4.1 Fluid–fluid lens under the combined effect of pressure driven and electroosmosis

First, flow visualization with fluorescent dye verified that under the combined effects of hydrodynamic and electroosmosis, the interfaces between the cladding fluids and the core fluid have an optically smooth arc shape.

As mentioned above, Rhodamine B is diluted in the cladding fluids to indicate the interfaces between the cladding fluids and the core fluid. Rhodamine B is a water-soluble fluorescent dye, can be excited by green light (540 nm) and emit red light with the maximum emission wavelength of 610 nm. The fluorescent image is recorded by an epi-fluorescent attachment of type Nikon G-2E/C. The interface shape between the three fluids is measured using the recorded images and a customized image processing program written in MATLAB (Wu et al. 2004; Wu and Nguyen 2005). The program cancels the noise in the collected images with an adaptive noise-removal filter. The program also determines the pixel intensity values across the channel, which is normalized using $I^* = (I - I_{min})/(I_{max} - I_{min})$, where I, I_{max}, and I_{min} are the intensity values, its maximum value, and minimum value, respectively. The program calculates the position (y) based on the derivative of concentration (I) with respect to the distance y, can be taken by the formula of $(I_2^* - I_1^*)/(y_2 - y_1)$. The interface position is determined when dI^*/dy has a maximum value. Using the above method, the interface position for a specific position along flow direction can be determined. The interface shape can be obtained by changing the specific position along the flow direction.

The interface shapes under the different voltages are shown in Fig. 7. The zeta potential between PMMA and aqueous solution is 24.7 mV (Gao et al. 2007) and the permittivity of conduction fluid is 6.9×10^{-1} (C^2 N^{-1} m^{-2}) (Gao et al. 2007). Figure 7 also compared the measured interface shapes with the stream lines calculated using Eq. 10. The agreement between the extracted interface shape and fitting arcs (Eq. 10) confirms that the interface shapes in the circular chamber have an optically
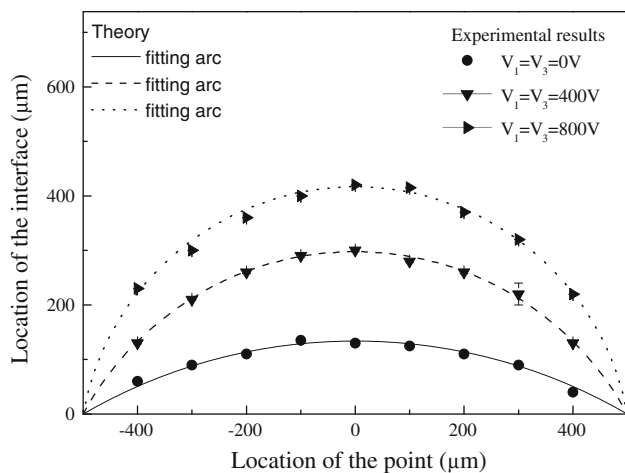
Fig. 7 The shape of the interface under the different voltages

smooth arc shape. The combined effect of hydrodynamic and electroosmosis can be used to control the optofluidic lens.
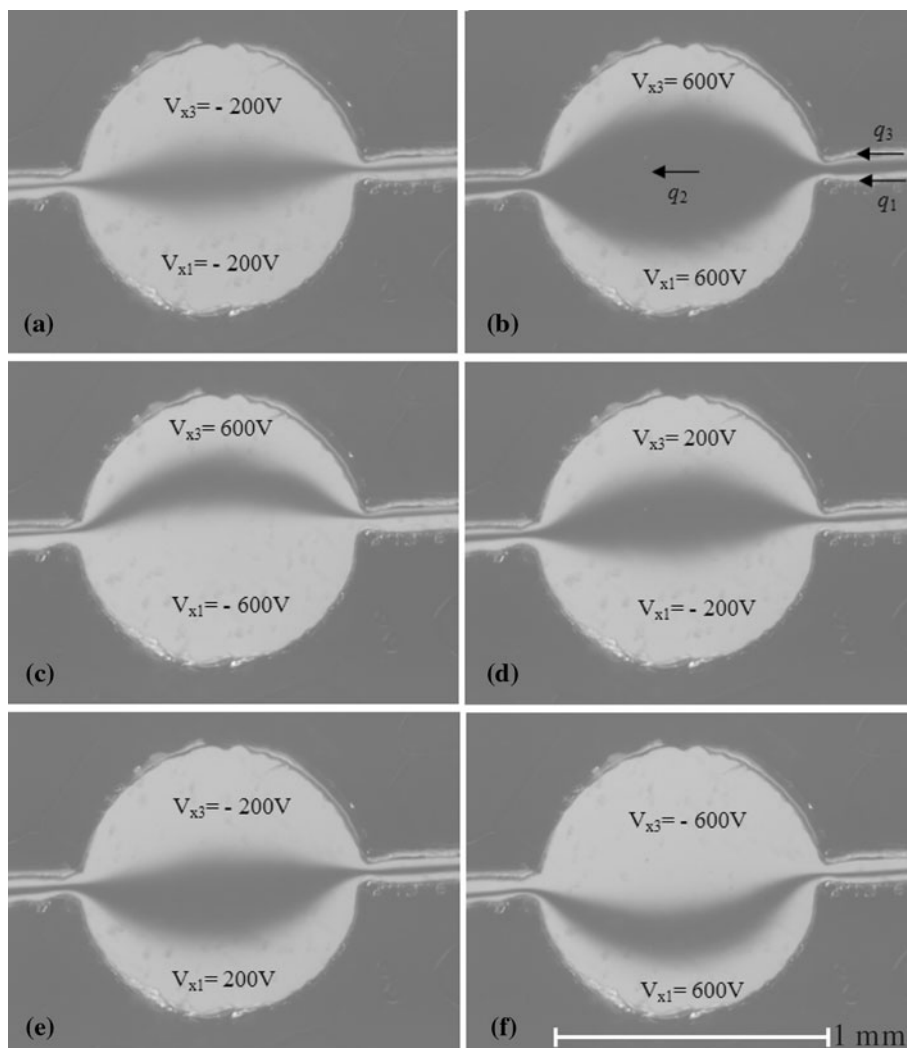
Figure 8 shows a series of different optofluidic lenses. The electroosmotic effect for controlling optofluidics lens is confirmed experimentally. Figure 8a–f shows that at a fixed flow rate, the curvatures of the interfaces (interfaces 1–2 and 3–2) can be modified according to the magnitudes and the polarities of the voltages.

If negative voltages are added to the cladding fluid 1 and the cladding fluid 3 simultaneously (Fig. 8a), the electroosmotic flows act against the pressure-driven flow. Consequently, q_1 encounters a larger resistance. q_1 appears to be more "viscous" due to the electroosmotic effect. Because of the same pressure drop along the microchannel and the fixed volumetric flow rate forced by the syringe pump, the more viscous fluid has to spread over a larger area, thus decreases the curvature of the interface. If positive voltages are added to the cladding fluid 1 and the cladding fluid 3 simultaneously (Fig. 8b), the electroosmotic velocity has the same direction with the flow direction and the cladding fluids flow faster. Due to the fixed volumetric flow rate forced by the syringe pump, the

Fig. 8 The fluid–fluid lenses based on the difference voltages ($q_1 = q_2 = q_3 = 0.05$ ml/h) **a** $V_{x1} = -200$ V; $V_{x3} = -200$ V; **b** $V_{x1} = 600$ V; $V_{x3} = 600$ V; **c** $V_{x1} = -600$ V; $V_{x3} = 600$ V; **d** $V_{x1} = -200$ V; $V_{x3} = 200$ V; **e** $V_{x1} = 200$ V; $V_{x3} = -200$ V; **f** $V_{x1} = 600$ V; $V_{x3} = -600$ V

cladding fluids have to spread over a smaller area, thus increase the curvature of the interface. Figure 8a, b shows that a symmetric biconvex lens can be achieved when symmetric voltages ($V_{x1} = V_{x3}$) are added to the cladding fluids.

When the applied voltages are different ($V_{x1} = -V_{x3}$), the curvatures of the interface 1 and the interface 3 have different values (Fig. 8c–f). Figure 5 defines the symbol of curvature and the type of the lens. When a negative voltage ($V_{x1} = -600$ V), and a positive voltage ($V_{x3} = 600$ V) are applied (Fig. 8c), the curvature of the interface 1 is negative and the curvature of the interface 3 is positive. Under the combined effect of a positive voltage and a negative voltage, a meniscus lens is formed (Fig. 8c–f). At moderate negative voltage strength, this technique allows the curvatures of both interfaces to be positive, hence a biconvex lenses or a plano-convex lens can be achieved (Fig. 8e–d).

The above results show that a negative voltage could decrease the curvature of the interface, while a positive voltage can increase the curvature of the interface. Under constant flow rates, the same voltage achieves symmetric biconvex lens only. Different voltages can form biconvex lens, plano-convex lens, and meniscus lens.

4.2 Symmetric biconvex lens: comparison between model and experiment

First, the symmetric voltages are added to the cladding fluids ($V_{x1} = V_{x3}$). Under the constant flow rates ($q_1 = q_2 = q_3 = 0.05$ ml/h) and the symmetric voltage, symmetric biconvex lenses are achieved. Figure 9 compares the dimensionless lens thickness ($\bar{T}_{h1}$) and the analytical results when symmetric voltages are applied. The dimensionless lens thickness ($\bar{T}_{h1}$) is defined in Eq. 37. A reasonable agreement is obtained. For the analytical solution, a reference length of $L_{ref} = 1000$ μm is taken; the zeta potential at the PMMA channel and aqueous NaCl is -24.4 mV as measured by the electroosmotic mobility method (Yan et al. 2006); the zeta potential at the interface between the aqueous glycerol and the NaCl solution is taken as -40 mV (Gu and Li 1998).

Figure 9 shows that symmetric voltages can be used to regulate the lens thickness. The dimensionless lens thickness $\bar{T}_{h1}$ decreases with the decrease of the voltages. The rate of change of $\bar{T}_{h1}$ is dependent on the polarity of the voltages. When positive voltages are added to the cladding fluids, the rate of change in the dimensionless lens thickness increases rapidly when the applied voltage increases from 0 to 1000 V; hence symmetric voltages can control the symmetric biconvex lens sensitively. When negative voltages (-1000 V $< V_{x1} < 0$ V) are added to the cladding fluids, the rate of change in dimensionless lens
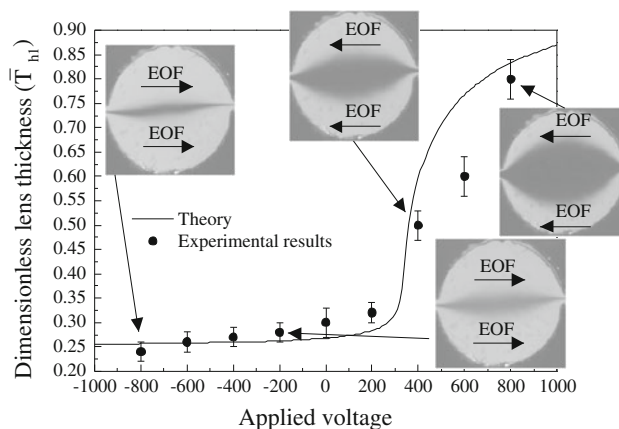

Fig. 9 Thickness of the lens verse applied voltage ($q_1 = q_2 = q_3 = 0.05$ ml/h, $L_{ref} = 1$ mm, $V_{x1} = V_{x3}$)
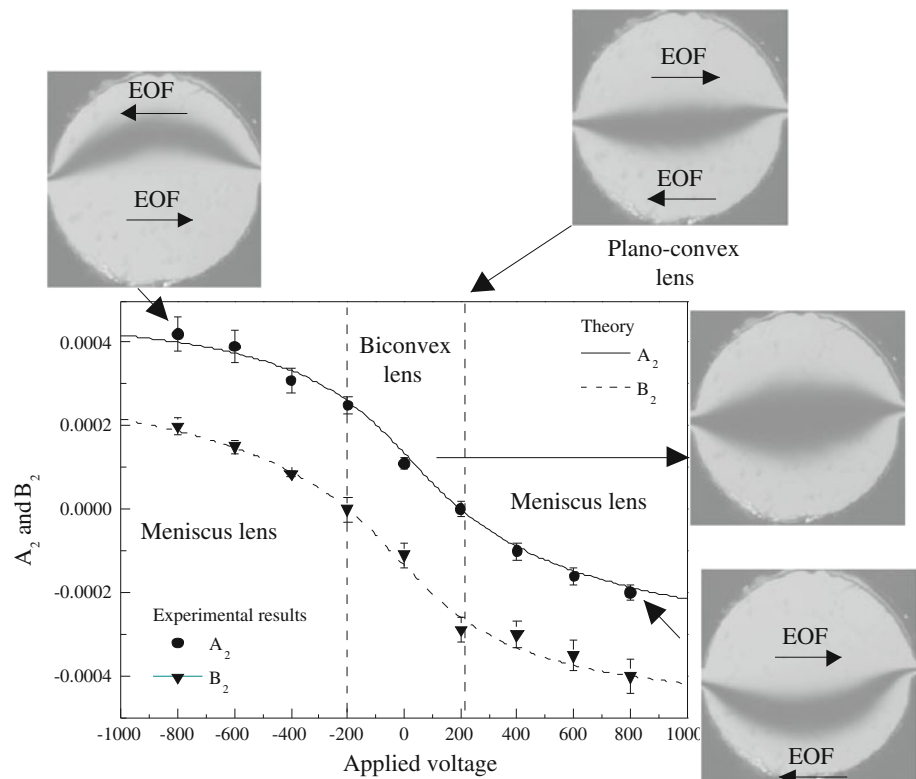
thickness $\bar{T}_{h1}$ decreases very slowly. The sensitivity can be improved by reducing the diameter of the circular chamber.

4.3 Biconvex lens, plano-convex lens, and meniscus lens: comparison between theoretical analysis and experiment

Figure 10 compares the measured curvature of the interface and the analytical results when the voltages have opposite polarity ($V_{x1} = -V_{x3}$). The results clearly show that the proposed model agrees well with the measurement. Figure 10 shows that under constant flow rates, different optofluidic lenses can be achieved but a combination of the positive and negative voltages is needed. If there is no voltage, the flow is purely pressure driven. If the cladding flows have the same rate, a symmetric biconvex lens is achieved. When different voltages are added to the cladding flows, κ_{1-2} and κ_{3-2} have different values. If the magnitude of the voltage is not high enough (e.g. -200 V $< V_{x1} < 200$ V), κ_{1-2} and κ_{3-2} are positive at the same time forming a biconvex. κ_{1-2} or κ_{3-2} decreases with the increase of voltages. A plano-convex lens is formed when $\kappa_{1-2} = 0$ or $\kappa_{3-2} = 0$ (e.g. $V_{x1} = -200$ V or $V_{x3} = -200$ V). When κ_{1-2} or κ_{3-2} is negative with an increasing magnitude of voltages (e.g. $|V_{x1}| > 200$ V), a meniscus lens is formed. The above results show that under a constant flow rate, a biconvex lens, a plano-convex lens, and a meniscus lens can be accomplished. The control voltage can be further reduced with a lower flow rate (Gao et al. 2007).

Figure 11 shows that the dimensionless thickness of the optofluidics lens varies with the different voltage. The analytical solutions of three fluids flow are driven using Eqs. 45–50. B_1, B_2, A_1, and A_2 are defined in Fig. 4. If the flow rate conditions are specified, the system of Eqs. 45–50 can be solved by the Newton–Raphson method to

Fig. 10 A_2 and B_2 with different voltages ($q_1 = q_2 = q_3 = 0.05$ ml/h, $L_{ref} = 1$ mm, $V_{x1} = -V_{x3}$)

determine the values of B_1, B_2, A_1, and A_2. The experiment results are measured using the recording results by CCD camera. Under the same flow rates, the dimensionless thickness has the maximum value without the voltage; it decreases with the increasing voltage. The analytical solution has a good agreement with the experimental results.

5 Conclusions

This paper presents the analytical model of a liquid-core liquid-cladding optofluidics lens tunable by the combined effect of hydrodynamics and electroosmosis. In this lens, an electrically conducting liquid is used as the cladding fluids, and the core fluid is non-conducting. Voltages are added to the cladding fluids. Under the constant flow rates, the theory of two-dimensional dipole flow in a circularly bounded domain and the theory of the electric field outside the parallel plat capacitor are used to predict the curvature of the interface. The above analytical model is validated by experimental results. In the experiments, a test device with a circular lens chamber with a 2-mm diameter and a 250-μm height is fabricated in PMMA using the thermal bounding method; two cladding fluids (aqueous NaCl) and the core fluid (poly (dimethylsiloxane)) are introduced by
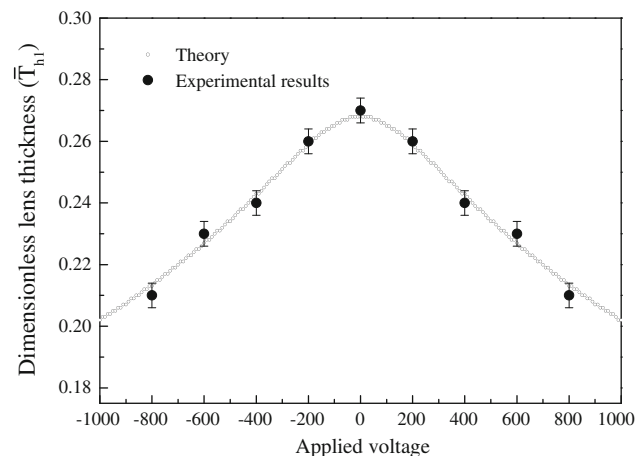

Fig. 11 Thickness of the lens with different voltages ($q_1 = q_2 = q_3 = 0.05$ ml/h, $L_{ref} = 1$ mm, $V_{x1} = -V_{x3}$)

syringe pumps to the circular domain. External electric fields are applied on the two cladding fluids. The results show that the interfaces between the cladding fluids and the core fluid are optically smooth arc-shape under the combined effect of hydrodynamic and electroosmosis. Under the constant flow rates, the symmetric voltages result in a symmetric biconvex lens only, while asymmetric voltages form biconvex lens, plano-convex lens, and meniscus lens. The experimental results agree well with the analytical model.

References

Camou S, Fujita H, Fujii T (2003) PDMS 2D optical lens integrated with microfluidic channels: principle and characterization. Lab Chip 3(1):40–45

Dino DC (2009) Inertial microfluidics. Lab Chip 9(21):3038–3046

Dong L, Jiang H (2008) Selective formation and removal of liquid microlenses at predetermined locations within microfluidics through pneumatic control. J Microelectromech Syst 17(2): 381–392

Gao Y, Wang C, Wong TN, Yang C, Nguyen NT, Ooi KT (2007) Electro-osmotic control of the interface position of two-liquid flow through a microchannel. J Micromech Microeng 17(2): 358–366

Gu Y, Li D (1998) The ζ-potential of silicone oil droplets dispersed in aqueous solutions. J Colloid Interface Sci 206(1):346–349

Kohlheyer D, Besselink GAJ, Lammertink RGH, Schlautmann S, Unnikrishnan S, Schasfoort RBM (2005) Electro-osmotically controllable multi-flow microreactor. Microfluid Nanofluid 1(3):242–248

Koplik J, Redner S, Hinch EJ (1994) Tracer dispersion in planar multipole flows. Phys Rev E 50(6):4650–4671

Li H, Wong TN, Nguyen NT (2009) Electroosmotic control of width and position of liquid streams in hydrodynamic focusing. Microfluid Nanofluid 7:489–497

Liu Y, Zeng X, Dong L, Jiang H (2009) Enhancing lab-on-a-chip performance via tunable parallel liquid mircolens arrays. Proceedings of SPIE - The International Society for Optical Engineering

Manz A, Effenhauser CS, Burggraf N, Harrison DJ, Seiler K, Fluri K (1994) Electroosmotic pumping and electrophoretic separations for miniaturized chemical analysis systems. J Micromech Microeng 4(4):257–265

Mao X, Waldeisen JR, Juluri BK, Huang TJ (2007) Hydrodynamically tunable optofluidic cylindrical microlens. Lab Chip 7(10): 1303–1308

Mao X, Juluri BK, Lin SC, Shi J, Lapsley MI, Huang TJ (2008) In-plane tunable optofluidic microlenses. LEOS Summer Topical Meeting

Mao X, Lin SCS, Lapsley MI, Shi J, Juluri BK, Huang TJ (2009) Tunable Liquid Gradient Refractive Index (L-GRIN) lens with two degrees of freedom. Lab Chip 9(14):2050–2058

Nguyen NT (2010) Micro optofluidic lenses—a review. Biomicrofluidics 4:031501

Psaltis D, Quake SR, Yang C (2006) Developing optofluidic technology through the fusion of microfluidics and optics. Nature 442(7101):381–386

Ren H, Liu L (2007) Fringe field effects of finite-size parallel electrodes. Opto-Electronic Engineering 34(7):102–106

Ren L, Escobedo C, Li D (2001) Electroosmotic flow in a microcapillary with one solution displacing another solution. J Colloid Interface Sci 242(1):264–271

Rosenauer M, Vellekoop MJ (2009) 3D fluidic lens shaping—a multiconvex hydrodynamically adjustable optofluidic microlens. Lab Chip 9(8):1040–1042

Shi J, Stratton Z, Lin SCS, Huang H, Huang TJ (2010) Tunable optofluidic microlens through active pressure control of an air-liquid interface. Microfluid Nanofluid 9(2–3):313–318

Sinton D, Li D (2003) Electroosmotic velocity profiles in microchannels. Colloids Surf A 222(1–3):273–283

Song C, Nguyen NT, Tan SH, Asundi AK (2009) Modelling and optimization of micro optofluidic lenses. Lab Chip 9(9):1178–1184

Song C, Nguyen NT, Tan SH, Asundi AK (2010) A tuneable micro-optofluidic biconvex lens with mathematically predictable focal length. Microfluid Nanofluid 9:889–896

Tang SKY, Stan CA, Whitesides GM (2008) Dynamically reconfigurable liquid-core liquid-cladding lens in a microfluidic channel. Lab Chip 8(3):395–401

Wang C, Gao Y, Nguyen NT, Wong TN, Yang C, Ooi KT (2005) Interface control of pressure-driven two-fluid flow in microchannels using electroosmosis. J Micromech Microeng 15(12): 2289–2297

Weigl BH, Bardell RL, Kesler N, Morris CJ (2001) Lab-on-a-chip sample preparation using laminar fluid diffusion interfaces computational fluid dynamics model results and fluidic verification experiments. Anal Bioanal Chem 371(2):97–105

Wenger J, Gerard D, Aouani H, Rigneault H (2008) Disposable microscope objective lenses for fluorescence correlation spectroscopy using latex microspheres. Anal Chem 80(17):6800–6804

Wolfe DB, Conroy RS, Garstecki P, Mayers BT, Fischbach MA, Paul KE, Prentiss M, Whitesides GM (2004) Dynamic control of liquid-core/liquid-cladding optical waveguides. Proc Natl Acad Sci USA 101(34):12434–12438

Wu Z, Nguyen NT (2005) Rapid mixing using two-phase hydraulic focusing in microchannels. Biomed Microdevices 7(1):13–20

Wu Z, Nguyen NT, Huang X (2004) Nonlinear diffusive mixing in microchannels: theory and experiments. J Micromech Microeng 14(4):604–611

Yan D, Nguyen NT, Yang C, Huang X (2006) Visualizing the transient electroosmotic flow and measuring the zeta potential of microchannels with a micro-PIV technique. J Chem Phys 124(2): 021103

Yaws CL (2003) Yaws' handbook of thermodynamic and physical properties of chemical compounds: physical, thermodynamic and transport properties for 5, 000 organic chemical compounds. Knovel, New York, USA